

Site-bond percolation of heteronuclear dimers irreversibly deposited on square lattices

P. M. Centres and A. J. Ramirez-Pastor

Departamento de Física, Instituto de Física Aplicada (INFAP), Universidad Nacional de San Luis-CONICET, Ejército de Los Andes 950, D5700HHW, San Luis, Argentina

M. C. Gimenez*

IFEG, CONICET, FaMAF, UNC, Córdoba, Argentina

(Received 25 October 2017; revised manuscript received 28 November 2017; published 26 December 2017)

A generalization of the site-bond percolation problem was studied, in which pairs of neighboring sites (site dimers) and bonds are occupied irreversibly, randomly, and independently on homogeneous square surfaces. A dimer is composed of two segments and occupies two adjacent sites. Each segment can be either a conductive segment (segment type *A*) or a nonconductive segment (segment type *B*). Two types of dimers are considered, *AA* and *AB*, and the connectivity analysis is carried out by accounting only for the conductive segments (segments type *A*) in combination with bonds. For the combination of dimers and bonds, two different criteria were analyzed: the union or the intersection between the adsorbed percolating particles and the bonds. By means of numerical simulations and finite-size scaling analysis, the complete phase diagram separating a percolating from a non-percolating region was determined.

DOI: [10.1103/PhysRevE.96.062136](https://doi.org/10.1103/PhysRevE.96.062136)**I. INTRODUCTION**

The percolation problem is one of the central problems in statistical mechanics, and the activity in this field is still growing [1–9]. Usually, the percolation model in a lattice is classified into two categories, namely, site model and bond model [6]. In the site (bond) model, sites (bonds) of a lattice are randomly occupied with a probability p_s (p_b) or empty (nonoccupied) with a probability $1 - p_s$ ($1 - p_b$). Nearest-neighboring occupied sites (bonds) form structures called clusters.

The main idea of the classical percolation theory is based on finding the minimum concentration of elements (sites or bonds) for which a cluster extends from one side of the system to the other [6]. This particular value of concentration rate is named critical concentration or percolation threshold and determines a phase transition in the system. The percolation transition is then a geometrical phase transition where the critical concentration separates a phase of finite clusters from a phase where a macroscopic, spanning, or infinite cluster is present. This geometric transition is a second-order phase transition and can be characterized by well-defined critical exponents.

Some real physical systems, however, have blockage in both sites and bonds, where occupied bonds act as communication links between occupied sites. The sol-to-gel transition (gelation) of polymers [10] is considered to be a prototype of this kind of problem. In this case, bonds represent chemical bonds, occupied sites represent monomers, and empty sites represent solvent molecules. In general, these systems can be modeled by assuming that both sites and bonds are randomly and independently occupied with occupancy fractions p_s and p_b , respectively. The occupation of sites and bonds are entirely independent and simultaneous processes. Then, it is possible to define two different site-bond percolation models: *site and bond* ($S \cap B$) and *site or bond* ($S \cup B$) percolation. In $S \cap B$ ($S \cup B$),

two points are said to be connected if a sequence of occupied sites and (or) bonds joins them. Thus, in $S \cap B$, a cluster is considered to be a set of occupied bonds and sites in which the bonds are joined by occupied sites, and the sites are joined by occupied bonds. In $S \cup B$, a bond or site contributes to cluster connectivity independently of the occupation of its endpoints.

In the case of $S \cap B$ site-bond percolation, the problem has many applications in different fields and has been studied in a wide variety of geometries [11–18]. Thus, the model was mentioned at first by Frisch and Hammersley [11]. Agrawal *et al.* [12] and Nakanishi and Reynolds [13] showed, by using a series method and position-space renormalization group, respectively, that the critical exponents of pure site percolation are also valid for site-bond percolation. Later, Yanuka and Englman [14] proposed an equation for the critical curve separating the sol-to-gel transition in the site-bond percolation model, for square, triangular, simple cubic and face-centered cubic (fcc) lattices. More recently, Tarasevich and van der Marck [15] presented a very complete and systematic study, where site-bond percolation thresholds were calculated by means of numerical simulations in many lattices in two to five dimensions. On the other hand, the $S \cap B$ model has been treated in the literature for square [16], triangular [17], and simple cubic [18] lattices.

More general percolation problems can be formulated by including deposition of elements occupying more than one site (multiple occupation of sites or multisite occupancy). The dimer is the simplest case of an extended object and contains all the properties of the multisite occupancy problem. In this framework, a generalization of the standard site-bond percolation problem, in which pairs of nearest-neighbor sites (site dimers) and pairs of nearest-neighbor bonds (bond dimers) are independently occupied, was studied on a square lattice [19]. The complete phase diagram of the system was obtained, showing significant differences with respect to the classical site-bond percolation phase diagram. The study in Ref. [19] was recently extended to triangular lattices [20].

*cgimenez@famaf.unc.edu.ar

The dimer problem was also addressed by Harder *et al.* [21], who investigated the formation of dimers on a surface to describe the nonlinear dependence of transport properties on composition in mixed-alkali ionic conductors. Holloway [22] studied the problem of site percolation on a diamond lattice occupied by a mixture of monatomic and diatomic species. The results allowed us to understand some of the features of the alloys of Ge with groups III–V semiconductors. Along the same lines, Gao *et al.* [23] investigated the process of dissociative adsorption of dimers and studied the percolating properties of dissociated monomers as a function of both the concentration of dimers and the dissociation probability. A phase diagram separating a percolating from a nonpercolating region was obtained.

In all of the papers mentioned above [19–23], the study was restricted to homonuclear dimers. However, real depositing particles generally present inhomogeneities due, for instance, to the presence of various chemical species, which can significantly affect the percolation properties of the system. In this sense, a site percolation model of linear k -mers with defects (k -mers containing a fraction of nonconducting defects) on an ideal square lattice was studied by Tarasevich *et al.* [24]. k -mer sizes ranging from 2 to 256 were considered. For each size k , a critical concentration of defects was found. Above this concentration, percolation is impossible. More recently, a site percolation model of defective (or heteronuclear) dimers was investigated by our group [25]. The presence of defects was introduced as two kinds of segments composing the dimers: type A (percolating) and type B (nonpercolating). Different cases were analyzed, according to the sequence of deposition of the particles, the types of dimers involved in the process, and the degree of alignment of the deposited objects. The results were found to be consistent with those from Ref. [24].

The site percolation problem has also been studied for k -mers on lattices with defective sites [26,27] and bonds [28]. However, in the best knowledge of the authors, there is still a lack of systematic studies on $S \cap B$ and $S \cup B$ percolation in the presence of multiple occupation of sites and defects. The objective of this paper is to provide a thorough study in this direction. For this purpose, extensive numerical simulations have been performed to study the complete site-bond percolation problem of heteronuclear dimers composed of segments A and B . Two types of particles were considered: AA and AB . The model offers a simplified representation of the problem of percolation of defective (nonideal) particles, where the presence of defects in the system is simulated by introducing a mixture of conductive or ideal segments (A) and nonconductive or imperfect segments (B). The site-bond percolation model may also mimic, to a rough approximation, more general cases of amorphous surfaces, where some bonds have been removed and the connectivity varies from site to site.

The paper is organized as follows: the model and simulation scheme are described in Sec. II. The calculation of the percolation thresholds and the resulting phase diagram is reported in Sec. III. The analysis of results obtained by using finite size scaling theory is presented in Sec. IV. The main purpose of this section is to test the universality of the problem by determining the numerical values of the critical exponents of the phase transition. Finally, conclusions are given in Sec. V.

II. MODEL AND CALCULATION METHOD

A. The model

Let us consider a surface represented by a two-dimensional square lattice of $M = L \times L$ sites with periodic boundary conditions. Two types of depositing objects are considered: site dimers and bonds. A site dimer is composed by two units, and occupies two adjacent lattice sites. Thus, a site is occupied by one dimer unit, or is empty. Each unit can be either a conductive segment (segment type A) or a nonconductive segment (segment type B). Two types of dimers have been considered: AA and AB ; and the connectivity analysis is carried out by accounting only for the conductive segments (segments type A).

Starting from an initially empty lattice, site dimers and bonds are independently deposited. The process is done in two stages. First, the dimers are deposited randomly, sequentially, and irreversibly on the lattice. The process is the following:

- (1) One lattice site i is chosen at random.
- (2) If the site i is empty, a second site is randomly selected from its four neighbors.
- (3) If both sites are unoccupied, a dimer (AA or AB) is deposited on those two sites. Otherwise, the attempt is rejected. The sequence (1)–(3) is called elemental deposition step (EDS), and corresponds to the well-known conventional dimer filling problem [29–31].
- (4) First, EDSs are repeated until the desired concentration θ_{AA} of AA dimers is reached; and second, EDSs are repeated until the desired concentration θ_{AB} of AB dimers is reached.

Equivalent configurations can be obtained by initially depositing all dimers on the lattice up to desirable total concentration $\theta_T = \theta_{AA} + \theta_{AB}$, and then randomly differentiating these dimers on AB and AA types according to their concentration. We verify that jamming and percolation properties are the same (within the numerical accuracy) for both deposition algorithms. The details of this analysis are given in the Appendix.

Due to the blocking of the lattice by the already randomly deposited objects, the limiting or jamming coverage, θ_j , is less than that corresponding to the close packing ($\theta_j < 1$). Consequently, the total site coverage $\theta_T = \theta_{AA} + \theta_{AB}$ ranges from 0 to θ_j . In the case of square lattices, the value of the jamming coverage for the conventional dimer filling problem is $\theta_j = 0.9068$ [30,31].

In a second stage, the conductive bonds are randomly dropped on the free places (links) of the lattice. The procedure is iterated until N_b bonds are deposited and the desired concentration ($\theta_b = N_b/2L^2$) is reached.

Figure 1 schematically illustrates the system used in this work. In part (a), a typical configuration of site dimers and occupied bonds is shown. Solid circles, open circles, and thick lines represent A -dimer units, B -dimer units, and occupied bonds, respectively.

After the filling of the lattice with the site dimers and bonds, two criteria were taken into account for percolation: $S \cup B$ and $S \cap B$. In $S \cap B$ ($S \cup B$), two points are said to be connected if a sequence of occupied sites and (or) bonds joins them.

The $S \cap B$ model can be considered as a correlated bond percolation problem, or a pure site problem in which one replaces the bond by a site with two neighbors. On the

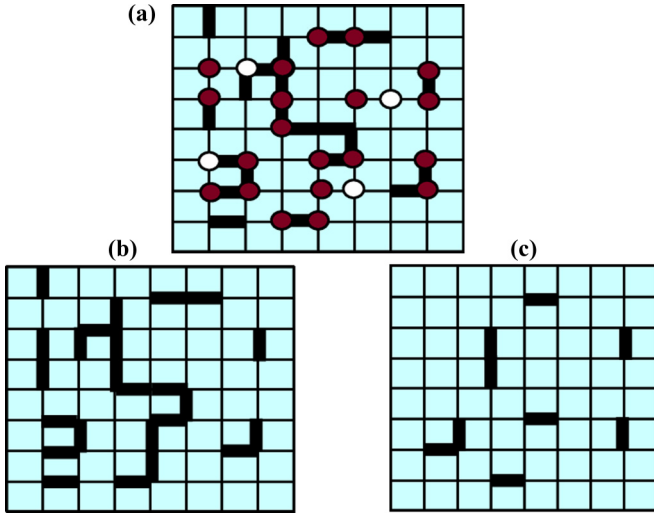


FIG. 1. (a) Schematic representation of a square lattice in which some site dimers and bonds have been deposited. Solid circles, open circles, and thick lines represent A -dimer units, B -dimer units, and occupied bonds, respectively. (b) Rules for the mapping $\mathbf{L} \rightarrow \mathbf{L}'$ from an original site-bond lattice \mathbf{L} (a) to an effective bond lattice \mathbf{L}' for $S \cup B$ model. (c) Same as part (b) for $S \cap B$ model.

other hand, the $S \cup B$ model can also be thought of as a bond problem, but not seem to be expressible as a pure site problem. Then, to calculate the percolation threshold, we can now think of a mapping $\mathbf{L} \rightarrow \mathbf{L}'$ from the original site-bond lattice \mathbf{L} to an effective bond lattice \mathbf{L}' where each bond and its endpoints sites of \mathbf{L} transforms into a bond one of \mathbf{L}' . The rules for the mapping depend on the studied problem. Thus, for *site-or-bond* percolation [see Fig. 1(b)]:

- (i) each occupied bond of \mathbf{L} transforms into an occupied bond one of \mathbf{L}' ;
- (ii) each empty bond with one or two empty endpoint sites of \mathbf{L} transforms into an empty bond in \mathbf{L}' ; and
- (iii) each empty bond with its occupied endpoint sites of \mathbf{L} transforms into an occupied bond of \mathbf{L}' .

On the other hand, for *site-and-bond* percolation [see Fig. 1(c)]:

- (i) each empty bond of \mathbf{L} transforms into an empty one of \mathbf{L}' ;
- (ii) each occupied bond with one or two empty endpoint sites of \mathbf{L} transforms into an empty bond in \mathbf{L}' ; and
- (iii) each occupied bond with its occupied endpoint sites of \mathbf{L} transforms into an occupied bond of \mathbf{L}' .

Once the mapping is completed, each percolating and non-percolating configuration in the effective lattice corresponds to a percolating and nonpercolating configuration in the original lattice. Then, the standard Hoshen and Kopelman algorithm [32] was applied for studying bond percolation on \mathbf{L}' .

B. Simulation scheme and finite-size scaling

As mentioned in Sec. I, the central idea of the percolation theory is based on finding the minimum coverage degree for which at least a cluster extends from one side to the opposite one of the system. This particular value of the coverage degree is named *percolation threshold* and determines a phase

transition in the system. In the present paper, given θ_{AA} and θ_{AB} , we look for the value of $\theta_b = \theta_{b,c}$ (percolation threshold) for which percolation occurs.

As the scaling theory predicts [33], the larger the system size to study, the more accurate the values of the threshold obtained. Thus, the finite-size scaling theory gives us the basis to achieve the percolation threshold and the critical exponents of a system with a reasonable accuracy. For this purpose, the probability $R = R_L^X(\theta_{AA}, \theta_{AB}, \theta_b)$ that a lattice composed of $L \times L$ sites percolates at concentrations $(\theta_{AA}, \theta_{AB}, \theta_b)$ can be defined [6,34,35]. Here, the following definitions can be given according to the meaning of X : R_L^U is the probability of finding either a rightward **or** a downward percolating cluster. R_L^I is the probability of finding a percolating cluster both in rightward **and** in downward direction. Finally, $R_L^A = (R_L^U + R_L^I)/2$.

Each simulation run consists of the following steps: (a) the construction of the lattice for the desired fractions $(\theta_{AA}, \theta_{AB}, \theta_b)$ and the criteria of junction ($S \cup B$) or intersection ($S \cap B$), according to the scheme mentioned in previous section; and (b) the cluster analysis by using the Hoshen and Kopelman algorithm [32]. Thus, n runs of such two steps are carried out for obtaining the number m^X of them for which a percolating cluster is found. Then, $R_L^X = m^X/n$ is defined. In the present study, a set of $n = 100\,000$ independent samples are numerically prepared for each model ($S \cup B$ and $S \cap B$), for each set of concentrations $(\theta_{AA}, \theta_{AB}, \theta_b)$ and lattice size L ($L = 128, 192, 256, 320, 384$). From the point of view of calculations, we set θ_{AA} and θ_{AB} , and vary θ_b .

In addition to the different probabilities $R_L^X(\theta_{AA}, \theta_{AB}, \theta_b)$, the percolation order parameter ($P = \langle S_L \rangle / M$) [36,37] and the susceptibility ($\chi = [\langle S_L^2 \rangle - \langle S_L \rangle^2] / 2L^2$) have been measured for each model, where S_L is the size of the largest cluster and $\langle \dots \rangle$ means an average over simulation runs.

III. PERCOLATION THRESHOLDS: SITE-BOND PERCOLATION PHASE DIAGRAM

As already explained, percolation is determined for 10^5 runs for each concentration $(\theta_{AA}, \theta_{AB}, \theta_b)$, on each lattice size L , for each model ($S \cup B$ and $S \cap B$), and for each percolation criterion ($X = U, I, A$).

The probabilities R_L^U , R_L^I and R_L^A are reported in Fig. 2(a) for a typical case: (a) $S \cup B$ model, $\theta_{AA} = 0.25$ and $\theta_{AB} = 0.64$. The fraction of bonds, θ_b , is varied during the simulation process. The corresponding percolation threshold $\theta_{b,c}$ can be obtained from the extrapolation of the positions $\theta_{b,c}^X(L)$ of the maxima of the slopes of R_L^X [6,34,35,38]. Thus, for each criterion ($U, I, \text{ or } A$),

$$\theta_{b,c}^X(L) = \theta_{b,c}^X(\infty) + A^X L^{-1/\nu}, \quad (1)$$

where A^X is a nonuniversal constant and ν is the critical exponent of the correlation length which will be taken as $4/3$ for the present analysis, since, as it will be shown in Sec. IV, our model belongs to the same universality class as random percolation [6].

Combining the three estimates for each case [$\theta_{b,c}^U(\infty)$, $\theta_{b,c}^I(\infty)$, and $\theta_{b,c}^A(\infty)$], the final value of $\theta_{b,c} \equiv \theta_{b,c}(\infty)$ can be obtained. Additionally, the maximum of the differences between $|\theta_{b,c}^U - \theta_{b,c}^A|$ and $|\theta_{b,c}^I - \theta_{b,c}^A|$ gives the error bar for

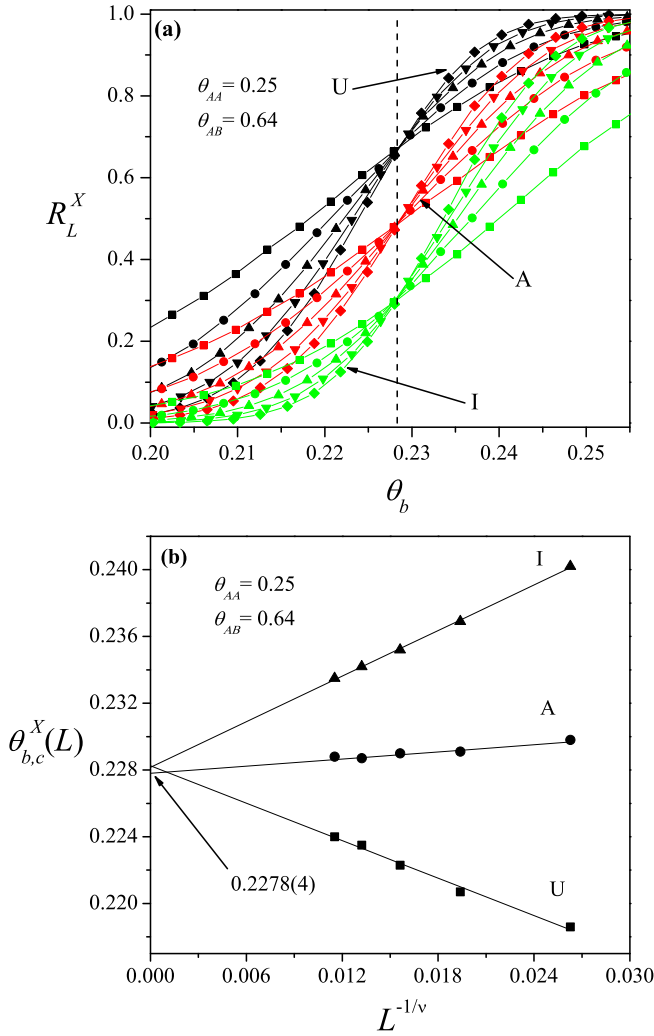


FIG. 2. (a) Fraction of percolating lattices R_L^X ($X = U, A, I$ as indicated) as a function of the bond concentration θ_b for $\theta_{AA} = 0.25$ and $\theta_{AB} = 0.64$ ($S \cup B$ model). For each criterion, different lattice sizes were considered: $L = 128$, squares; 192, circles; 256, up triangles; 320, down triangles; and 384, diamonds. (b) Extrapolation of $\theta_{b,c}^X(L)$ toward the thermodynamic limit [Eq. (1)] for the data shown in (a). Triangles, circles, and squares denote the values of $\theta_{b,c}^X(L)$, obtained by using the criteria I , A , and U , respectively.

each determination of $\theta_{b,c}$. Figure 2(b) shows this methodology for the data in Fig. 2(a). In this case, the value obtained was: $\theta_{b,c} = 0.2278(4)$.

The procedure in Fig. 2 was repeated for both models ($S \cup B$ and $S \cap B$), and different values of θ_{AA} and θ_{AB} . In addition, θ_{AA} and θ_{AB} must satisfy the jamming condition $0 \leq \theta_{AA} + \theta_{AB} \leq 0.9068$, where 0.9068 is the jamming coverage corresponding to dimers on square lattices [30,31]. Under these considerations, the complete phase diagram of the system was obtained. The results are shown in Fig. 3(a).

Let us start with the case of $S \cap B$ model [see top-right in Fig. 3(a)]. For a given value of θ_{AB} , a critical curve separating the percolating and nonpercolating regions is obtained. This curve varies between two limit points. The left extreme arises from the jamming condition $\theta_{AA}^{II} = \theta_j - \theta_{AB}$ and, consequently, θ_{AA}^{II} is the maximum possible value for

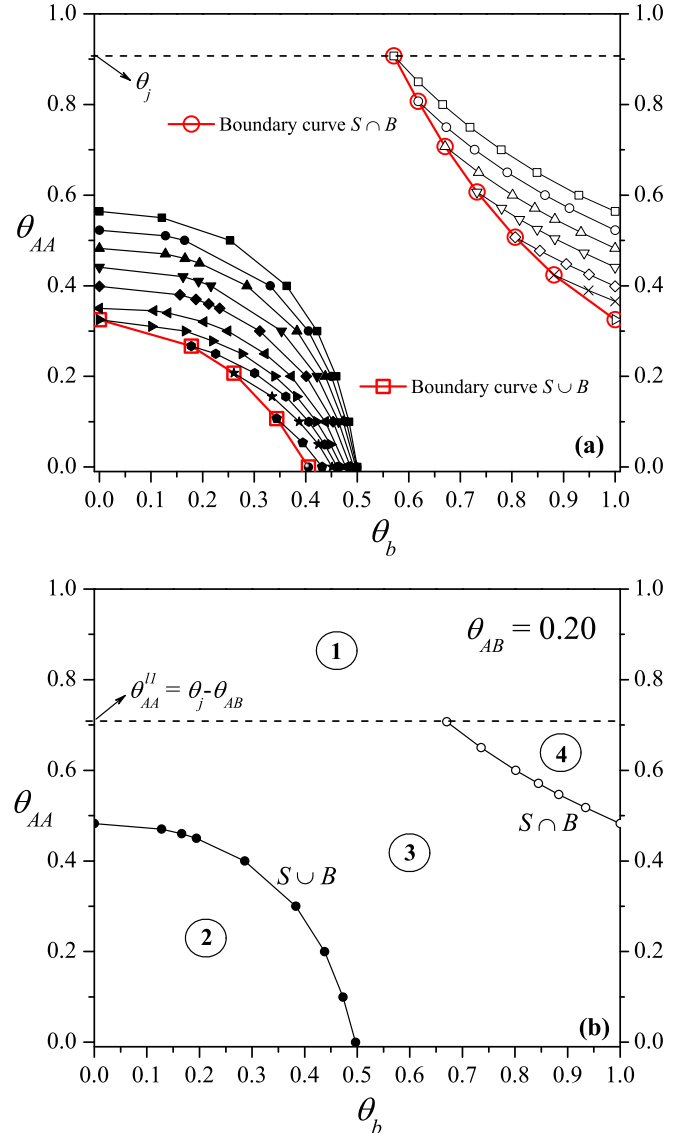


FIG. 3. (a) Percolation phase diagrams (in the θ_{AA} - θ_b parameter space) corresponding to site dimers and bonds independently deposited on square lattices: $S \cup B$ model (solid symbols) and $S \cap B$ model (open symbols). Different curves correspond to different values of θ_{AB} : 0, squares; 0.10, circles; 0.20, up triangles; 0.30, down triangles; 0.40, diamonds; 0.48, crosses; 0.50, left triangles; 0.58, right triangles; 0.64, hexagons; 0.70, stars; 0.80, pentagons; and 0.90, spheres. The size of the points is larger than the corresponding error bars. (b) Phase diagram corresponding to $\theta_{AB} = 0.20$. Percolating and nonpercolating regions are indicated in the figure. Region 1: forbidden region ($\theta_{AA} > \theta_{AA}^{II} = \theta_j - \theta_{AB}$); region 2: nonpercolating region for $S \cap B$ and $S \cup B$ models; region 3, percolating region for $S \cup B$ model, and nonpercolating region for $S \cap B$ model; and region 4, percolating region for $S \cap B$ and $S \cup B$ models.

θ_{AA} . The critical fraction of bonds corresponding to θ_{AA}^{II} will be denoted as θ_b^{II} . The points $[\theta_{AA}^{II}, \theta_b^{II}]$ are indicated as big open circles in Fig. 3(a).

On the other hand, the right extreme of each critical curve is $[\theta_{AA}^I, \theta_b = 1]$, where θ_{AA}^I represents the percolation threshold of the standard site percolation model of AA and AB dimers. This problem was studied in Ref. [25]. In the case of $\theta_{AB} = 0$,

only AA dimers are present in the system and θ_{AA}^{r1} corresponds to the already known percolating threshold of 0.564(2) for isotropic dimers on square lattices [39,40]. As θ_{AB} increases, the value of θ_{AA}^{r1} diminishes up to $\theta_{AA}^{r1} \approx 0.32$ for $\theta_{AB} \approx 0.58$. It is important to clarify here that θ_{AB} can vary between 0 and approximately 0.58. As shown in Ref. [25], there exists a critical concentration of AB dimers ($\theta_{AB} \approx 0.58$). Above this concentration, percolation is impossible.

In the range ($\theta_{AA}^{r1} < \theta_{AA} < \theta_{AA}^{l1}$), the percolation thresholds are obtained by following the scheme discussed in Fig. 2. The resulting curves are shown in Fig. 3(a). Each curve, corresponding to a different value of θ_{AB} , divides the space of allowed values of θ_{AA} and θ_b in a nonpercolating region (region below the critical curve) and a percolating region (region above the critical curve). In addition, as discussed in previous paragraphs, all critical curves are contained between two limit lines: the line joining the points $[\theta_{AA}^{l1}, \theta_b^{l1}]$ (boundary $S \cap B$ curve, big open circles) and the line $\theta_b = 1$. Note that for the maximum value of $\theta_{AB} \approx 0.58$, the critical curve is reduced to only one point $[\theta_{AA} \approx 0.32, \theta_b = 1]$. This point is the intersection point of the two limit lines.

In the case of $S \cup B$ model [see bottom-left in Fig. 3(a)], two types of behavior are observed for the percolation curves depending on the values of θ_{AB} . For $\theta_{AB} \lesssim 0.58$, the left extremes of critical curves (θ_{AA}^{l2}) intersect the coordinate axis. In this case, θ_{AA}^{l2} represents the critical fraction of AA dimers for $\theta_b = 0$. At this condition ($\theta_b = 0$), $S \cup B$ model reduces to $S \cap B$ model with $\theta_b = 1$ and, consequently, $\theta_{AA}^{l2} = \theta_{AA}^{r1}$.

As $0.58 < \theta_{AB} \leq \theta_j$, percolation is impossible for $\theta_b = 0$, and a minimum fraction of bonds is needed for percolation. We will denote as θ_b^{l2} this fraction of bonds. To calculate θ_{AA}^{l2} , θ_{AA} is set to $\theta_j - \theta_{AB}$, and θ_b is varied according to the procedure in Fig. 2. The points $[\theta_{AA}^{l2} = \theta_j - \theta_{AB}, \theta_b^{l2}]$ are shown in Fig. 3(a) as big open squares.

Summarizing, the left extremes of the percolation curves for $S \cup B$ model $[\theta_{AA}^{l2}, \theta_b^{l2}]$ can be written as: (1) $\theta_{AA}^{l2} = \theta_{AA}^{r1}$ and $\theta_b^{l2} = 0$ for $\theta_{AB} \lesssim 0.58$; and (2) $\theta_{AA}^{l2} = \theta_j - \theta_{AB}$ and $\theta_b^{l2} > 0$ for $0.58 < \theta_{AB} \leq \theta_j$.

The right extremes of the $S \cup B$ percolation curves are obtained by setting $\theta_{AA} = 0$ and varying θ_{AB} between 0 and θ_j . These limit points will be denoted as $[\theta_{AA}^{r2} = 0, \theta_b^{r2}]$. In the case of $\theta_{AB} = 0$, the critical fraction of bonds is equal to 0.5. This value represents the well-known percolation threshold for the standard bond percolation model on square lattices [6]. In general, θ_b^{r2} diminishes with θ_{AB} , being $\theta_b^{r2} \approx 0.4053$ in the limit of $\theta_{AB} = \theta_j$.

Once the left and right extremes are determined for each value of θ_{AB} , the intermediate points of the $S \cup B$ critical curves are calculated by varying θ_{AA} between 0 and θ_{AA}^{l2} . The resulting curves are shown in Fig. 3(a) as open symbols. The region below (above) the critical curve is the nonpercolating (percolating) region. In the case of $\theta_{AB} = \theta_j$, the percolation curve is reduced to only one point $[\theta_{AA} = 0, \theta_b \approx 0.4053]$.

Figure 3(b) allows for a better visualization of the percolating and nonpercolating regions. In the figure, the phase diagram corresponding to $\theta_{AB} = 0.20$ is shown. Four regions were indicated in the phase diagram. Region 1: forbidden region ($\theta_{AA} > \theta_{AA}^{l1} = \theta_j - \theta_{AB}$); region 2: nonpercolating region for $S \cap B$ and $S \cup B$ models; region 3, percolating region for $S \cup B$ model, and nonpercolating region for $S \cap B$

model; and region 4, percolating region for $S \cap B$ and $S \cup B$ models.

The phase diagrams presented in Fig. 3(a) offer a simplified representation of the problem of percolation of heterogeneous particles (particles containing conductive and nonconductive segments) in amorphous solids, where the presence of defects in the system is simulated by introducing a fraction of defective (empty) bonds. In this context, the results obtained are very useful as a first tool to predict the behavior of a system governed by a large number of parameters.

IV. CRITICAL EXPONENTS AND UNIVERSALITY

In this section, the critical exponents ν , β , and γ will be calculated. Critical exponents are of importance because they describe the universality class of the system and allow for the understanding of the related phenomena.

The standard theory of finite-size scaling [6] allows for various efficient routes to estimate the critical exponent ν from simulation data. One of these methods is from the maximum of the function $dR_L^X/d\theta_b$,

$$\left(\frac{dR_L^X}{d\theta_b}\right)_{\max} \propto L^{1/\nu}. \quad (2)$$

In Fig. 4(a), $\log[(\frac{dR_L^X}{d\theta_b})_{\max}]$ has been plotted as a function of $\log[L]$ (note the log-log functional dependence) for two typical cases: (i) $S \cup B$ model, $\theta_{AA} = 0.25$ and $\theta_{AB} = 0.64$; and (ii) $S \cap B$ model, $\theta_{AA} = 0.52$ and $\theta_{AB} = 0.30$. According to Eq. (2), the slope of each line corresponds to $1/\nu$. As it can be observed, the slopes of the curves remains constant, being $\nu = 1.34(3)$ for case (i), and $\nu = 1.34(4)$ for case (ii).

Another alternative way for evaluating ν is from the divergence of the root mean square deviation of the threshold observed from their average values, ΔR_L^X ,

$$\Delta R_L^X \propto L^{-1/\nu}. \quad (3)$$

As an example of the validity of the last equation, the inset in Fig. 4(a) shows ΔR_L^X as a function of L (note de log-log scale) for the same cases in the main figure. According to Eq. (3), the slope of the line corresponds to $-1/\nu$. In this case, $\nu = 1.34(3)$ for $\theta_{AA} = 0.25$ and $\theta_{AB} = 0.64$ ($S \cup B$), and $\nu = 1.33(3)$ for $\theta_{AA} = 0.52$ and $\theta_{AB} = 0.30$ ($S \cap B$).

The study in Fig. 4(a) was repeated for different values of θ_{AA} and θ_{AB} , and the U , A , and I criteria. In all cases, the results obtained for ν coincide, within numerical errors, with the exact value of the critical exponent of the ordinary percolation, namely, $\nu = 4/3$ [6].

Once we know ν , the exponent γ can be obtained by scaling the maximum value of the susceptibility χ . According to the finite-size scaling theory [6], the behavior of χ at criticality is $\chi = L^{\gamma/\nu} \bar{\chi}(u)$, where $u = (\theta_b - \theta_{b,c})L^{1/\nu}$ and $\bar{\chi}$ is the corresponding scaling function. At the point where χ is maximal, $u = \text{const.}$ and $\chi_{\max} \propto L^{\gamma/\nu}$. Our data for χ_{\max} are shown in Fig. 4(b). The values obtained are $\gamma = 2.40(3)$ for $\theta_{AA} = 0.25$ and $\theta_{AB} = 0.64$ ($S \cup B$); and $\gamma = 2.40(4)$ for $\theta_{AA} = 0.52$ and $\theta_{AB} = 0.30$ ($S \cap B$). Simulation data are consistent with the exact value of the critical exponent of the ordinary percolation problem, $\gamma = 43/18$.

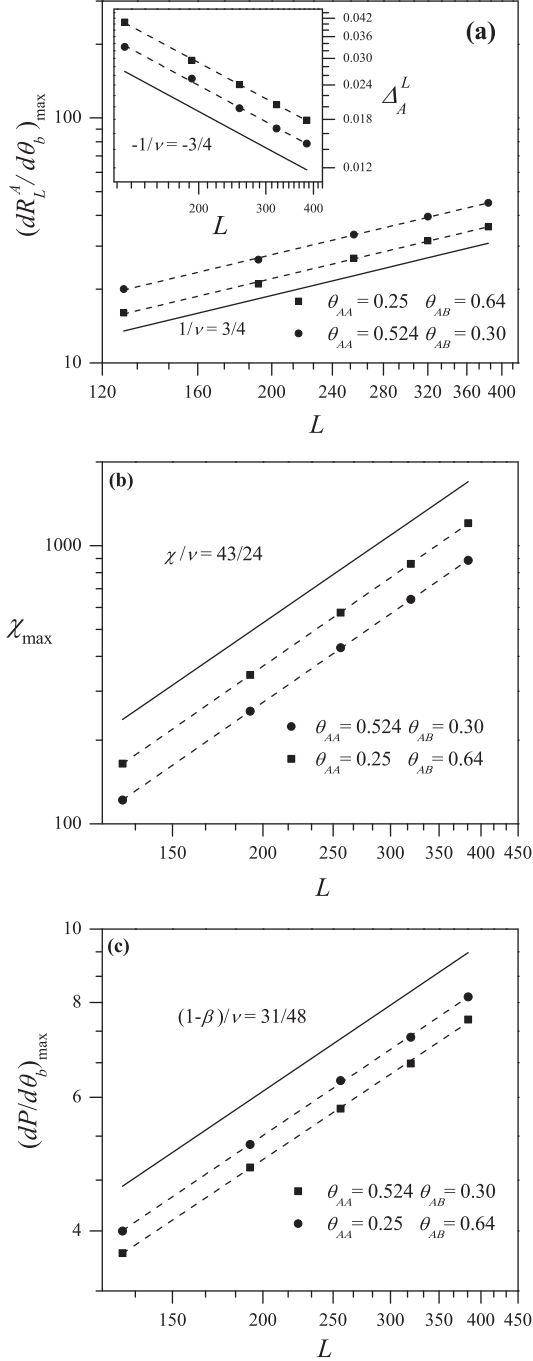


FIG. 4. (a) Log-log plot of $(dR_L^A/d\theta_b)_{\max}$ as a function of L for $S \cup B$ ($\theta_{AA} = 0.25$ and $\theta_{AB} = 0.64$) and $S \cap B$ ($\theta_{AA} = 0.52$ and $\theta_{AB} = 0.30$). According to Eq. (2) the slope of the curve corresponds to $1/\nu$. Inset: $\log \Delta_L^A$ as a function of L for the same case in the main figure. According to Eq. (3), the slope of the curve corresponds to $-1/\nu$. (b) Log-log plot of χ_{\max} as a function of L for the cases in part (a). The slope of each line corresponds to $\gamma/\nu = 43/24$. (c) Log-log plot of $(dP/d\theta_b)_{\max}$ as a function of L for the cases in parts (a) and (b). According to Eq. (5), the slope of each curve corresponds to $(1-\beta)/\nu = 31/48$.

On the other hand, the standard way to extract the exponent ratio β is to study the scaling behavior of P at criticality [6],

$$P = L^{-\beta/\nu} \bar{P}(u') \quad (4)$$

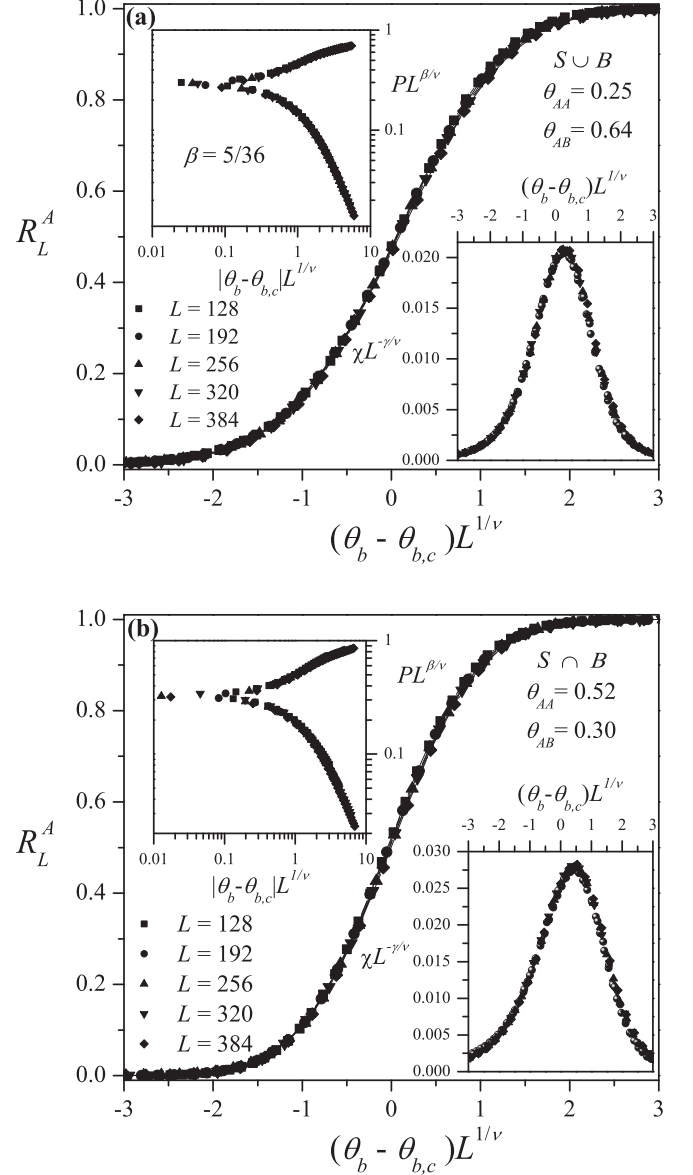


FIG. 5. Data collapsing of the percolation probability, R_L^A vs $(\theta_b - \theta_{b,c})L^{1/\nu}$. Upper left inset: data collapsing of the percolation order parameter, $PL^{\beta/\nu}$ vs $|\theta_b - \theta_{b,c}|L^{1/\nu}$. Bottom right inset: data collapsing of the susceptibility, $\chi L^{-\gamma/\nu}$ vs $(\theta_b - \theta_{b,c})L^{1/\nu}$. The plots were made using the exact percolation exponents $\nu = 4/3$, $\beta = 5/36$, and $\gamma = 43/18$. (a) $S \cup B$ model ($\theta_{AA} = 0.25$ and $\theta_{AB} = 0.64$), and (b) $S \cap B$ ($\theta_{AA} = 0.52$ and $\theta_{AB} = 0.30$).

where $u' = |\theta_b - \theta_{b,c}|L^{1/\nu}$ and \bar{P} is the scaling function. At the point where $dP/d\theta_b$ is maximal, $u = \text{const.}$ and

$$\left(\frac{dP}{d\theta_b}\right)_{\max} = L^{(-\beta/\nu+1/\nu)} \bar{P}(u') \propto L^{(1-\beta)/\nu}. \quad (5)$$

The scaling of $(dP/d\theta_b)_{\max}$ is shown in Fig. 4(c) for the cases in parts (a) and (b). From the slopes of the curves, the following values of β were obtained: $\beta = 0.14(2)$ for $\theta_{AA} = 0.25$ and $\theta_{AB} = 0.64$ ($S \cup B$); and $\beta = 0.13(2)$ for $\theta_{AA} = 0.52$ and $\theta_{AB} = 0.30$ ($S \cap B$). These results agree very well with the exact value of β for ordinary percolation, $\beta = 5/36$.

The values calculated for ν [Fig. 4(a)], γ [Fig. 4(b)], and β [Fig. 4(c)] clearly indicate that this problem belongs to the same universality class that the random percolation regardless the model ($S \cap B$ or $S \cup B$) and the values of θ_{AA} , θ_{AB} , and θ_b considered.

The scaling behavior can be further tested by plotting R_L^X versus $(\theta_b - \theta_{b,c})L^{1/\nu}$, $PL^{\beta/\nu}$ versus $|\theta_b - \theta_{b,c}|L^{1/\nu}$, and $\chi L^{-\gamma/\nu}$ versus $(\theta_b - \theta_{b,c})L^{1/\nu}$ and looking for data collapsing [6]. Using the values of $\theta_{b,c}$ calculated above and the exact values of the critical exponents of the ordinary percolation $\nu = 4/3$, $\beta = 5/36$, and $\gamma = 43/18$, we obtain an excellent scaling collapse for the cases discussed in the previous figures (see Fig. 5). This leads to independent controls and consistency checks of the values of all the critical exponents.

V. CONCLUSIONS

In the present work, the site-bond percolation problem for heteronuclear site dimers on square lattices has been addressed. The dimers are particles composed of two units and occupy two adjacent sites. Each unit can be either a conductive segment (segment type A) or a nonconductive segment (segment type B). Two types of dimers were considered: AA and AB ; and the connectivity analysis was carried out by accounting only for the conductive segments in combination with bonds.

Two distinct connectivity schemes, site-and-bond ($S \cap B$) and site-or-bond ($S \cup B$), were considered. In $S \cap B$, a cluster is considered to be a set of occupied bonds and sites in which the bonds are joined by occupied sites, and the sites are joined by occupied bonds. In $S \cup B$, a bond or site contributes to cluster connectivity independently of the occupation of its endpoints. Under these considerations, the percolation phase transitions occurring in the system were studied by using numerical simulations and finite-size scaling theory.

A wide variety of behaviors were observed depending on the scheme used ($S \cap B$ or $S \cup B$), and the values of the parameters of the model (θ_{AA} , θ_{AB} , and θ_b). From the point of view of calculations, we set θ_{AA} and θ_{AB} , and vary θ_b . The obtained phase diagram ($S \cap B$ and $S \cup B$ critical lines separating the percolating and nonpercolating regions) is presented for the first time in the literature. Its main characteristics are the following:

(1) The jamming coverage plays an important role in the system considered here. In fact, the curve $\theta_{AA} = \theta_j$ (where $\theta_j = 0.9068$ is the jamming coverage corresponding to dimers on square lattices [30,31]) determines the space of all the allowed values of θ_{AA} . The region above this curve corresponds to a forbidden region of the θ_{AA} -space. On the other hand, θ_b varies between 0 and 1.

(2) In the case of $S \cap B$ model, the percolation curves (obtained for different values of θ_{AB}) are contained between two limit lines: the line determined by the jamming condition $\theta_{AA} = \theta_j - \theta_{AB}$ and the line $\theta_b = 1$. θ_{AB} varies between 0 and ≈ 0.58 . As $\theta_{AB} = 0$, only AA dimers are present in the system, and the critical curve corresponds to the already known case of $S \cap B$ model for isotropic dimers on square lattices [39,40].

As $\theta_{AB} \approx 0.58$, the critical curve is reduced to only one point [$\theta_{AA} \approx 0.32, \theta_b = 1$]. This point is the intersection point of the two limit lines. $\theta_{AB} \approx 0.58$ is the critical concentration of defective AB dimers. Above this concentration, $S \cap B$ percolation is impossible.

(3) More complex is the situation for $S \cup B$ model. In this scheme, the percolation curves show two different behaviors depending on the values of θ_{AB} . For $\theta_{AB} \lesssim 0.58$, critical curves extend from the coordinate axis ($\theta_b = 0$) to the abscissa axis ($\theta_{AA} = 0$). As $0.58 < \theta_{AB} \leq \theta_j$, percolation is impossible for $\theta_b = 0$, and a minimum fraction of bonds is needed for percolation. This minimum fraction of bonds is calculated by setting $\theta_{AA} = \theta_j - \theta_{AB}$ (jamming condition). On the other hand, the intersection points between the critical curves and the abscissa axis are obtained by setting $\theta_{AA} = 0$ and varying θ_{AB} between 0 and θ_j . In the case of $\theta_{AB} = 0$, the critical fraction of bonds is equal to 0.5. This value represents the well-known percolation threshold for the standard bond percolation model on square lattices [6]. In the limit of $\theta_{AB} = \theta_j$, the critical fraction of bonds is equal to 0.4053. Then, the effect of the presence of defective dimers in the $S \cup B$ scheme could be summarized as follows. For $\theta_{AB} = 0$, the critical curve corresponds to the already known case of $S \cup B$ model for isotropic dimers on square lattices [19,39,40] and extends from $\theta_b = 0$ to $\theta_b = 0.5$. As θ_{AB} is increased, the range of values of θ_b for which percolation occurs is reduced. For the maximum possible value of the fraction of defective dimers $\theta_{AB} = \theta_j$, the percolation curve is reduced to only one point [$\theta_{AA} = 0, \theta_b \approx 0.4053$].

(4) The complete phase diagram presented in this work offers a simplified representation of the problem of percolation of heterogeneous particles (particles containing conductive and nonconductive segments) in amorphous solids, where the presence of defects in the system is simulated by introducing a fraction of defective (empty) bonds. In this context, the results obtained are very useful as a first tool to predict the behavior of a system governed by a large number of parameters.

Finally, the accurate determination of the critical exponents ν , β and γ revealed that, regardless the model ($S \cap B$ or $S \cup B$) and the values of θ_{AA} , θ_{AB} , and θ_b considered, the problem belongs to the same universality class as two-dimensional random percolation model.

ACKNOWLEDGMENTS

This work was supported in part by CONICET (Argentina) under Project No. PIP 112-201101-00615; Universidad Nacional de San Luis (Argentina) under Project No. 03-0816; and the National Agency of Scientific and Technological Promotion (Argentina) under Project No. PICT-2013-1678. The numerical work were done using the BACO parallel cluster (composed by 70 PCs each with an Intel i7-3370/2600 processor) located at Instituto de Física Aplicada, Universidad Nacional de San Luis - CONICET, San Luis, Argentina. Financial support from Secyt-UNC and Foncyt is also acknowledged.

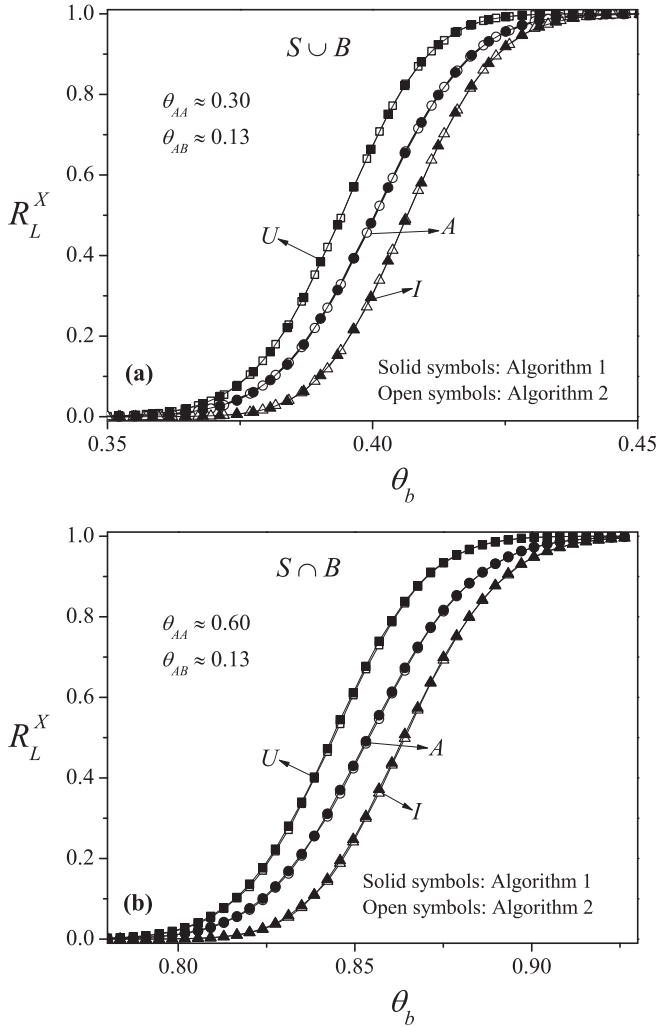


FIG. 6. (a) Fraction of percolating lattices R_L^X ($X = U, A, I$ as indicated) as a function of the bond concentration θ_b for $L = 128$, $\theta_{AA} \approx 0.30$, and $\theta_{AB} \approx 0.13$ ($S \cup B$ model). (b) Same as part (a) for $\theta_{AA} \approx 0.60$ and $\theta_{AB} \approx 0.13$ ($S \cap B$ model). In all cases, the numerical values were calculated on a set of 100 000 independent samples. Solid (open) symbols represent data obtained using Algorithm 1 (2).

APPENDIX

Here we provide the details of the deposition algorithms discussed in the manuscript.

Dimer deposition mechanisms

The dimers are deposited randomly, sequentially, and irreversibly on the lattice. The process is the following:

- (1) One lattice site i is chosen at random.
- (2) If the site i is empty, a second site is randomly selected from its four neighbors.
- (3) If both sites are unoccupied, a dimer (AA or AB) is deposited on those two sites. Otherwise, the attempt is rejected. The sequence (1)–(3) is called elemental deposition step (EDS), and it corresponds to the well-known conventional dimer-filling problem [29–31].

(4) First, EDSs are repeated until the desired concentration θ_{AA} of AA dimers is reached; and second, EDSs are repeated until the desired concentration θ_{AB} of AB dimers is reached. This algorithm will be called Algorithm 1.

Equivalent configurations can be obtained by initially depositing all dimers on the lattice up to desirable total concentration $\theta_T = \theta_{AA} + \theta_{AB}$, and then randomly differentiating these dimers on AB and AA types according to their concentration. This algorithm will be called Algorithm 2.

The jamming properties depend only on the structure of the deposited particles and, consequently, are not affected by the particular sequence in which the AA and AB dimers are deposited on the lattice. With respect to the percolation properties, we verified that both deposition algorithms are equivalent. This situation is clearly reflected in Fig. 6, where the probabilities R_L^U , R_L^I , and R_L^A are reported for two typical cases: (a) $\theta_{AA} \approx 0.30$ and $\theta_{AB} \approx 0.13$ ($S \cup B$ model); and (b) $\theta_{AA} \approx 0.60$ and $\theta_{AB} \approx 0.13$ ($S \cap B$ model). In all cases, the numerical values were calculated on a set of 100 000 independent samples with $L = 128$. Solid (open) symbols represent data obtained using Algorithm 1 (2). The excellent agreement observed between the curves corresponding to Algorithm 1 and Algorithm 2 supports the equivalence between both deposition mechanisms [41]. Similar results were obtained for several values of θ_{AA} , θ_{AB} and L . Due to computational efficiency considerations, Algorithm 1 will be used in this paper.

[1] J. M. Hammersley, *Proc. Camb. Phil. Soc.* **53**, 642 (1957).
 [2] J. W. Essam, *Rep. Prog. Phys.* **43**, 833 (1980).
 [3] R. Zallen, *The Physics of Amorphous Solids* (John Wiley & Sons, New York, 1983).
 [4] *Percolation Structures and Processes*, Annals of the Israel Physical Society Vol. 5, edited by G. Deutscher, R. Zallen, and J. Adler (Hilger, Bristol, 1983).
 [5] M. Sahimi, *Applications of Percolation Theory* (Taylor & Francis, London, 1992).
 [6] D. Stauffer and A. Aharony, *Introduction to Percolation Theory* (Taylor & Francis, London, 1994).
 [7] G. Grimmett, *Percolation* (Springer-Verlag, Berlin, 1999).
 [8] B. Bollobás and O. Riordan, *Percolation* (Cambridge University Press, New York, 2006).

[9] M. E. J. Newman, *Networks: An Introduction* (Oxford University Press, Oxford, UK, 2010).
 [10] A. Coniglio, H. E. Stanley, and W. Klein, *Phys. Rev. Lett.* **42**, 518 (1979).
 [11] H. L. Frisch and J. M. Hammersley, *J. Soc. Ind. Appl. Math.* **11**, 894 (1963).
 [12] P. Agrawal, S. Render, P. J. Reynolds, and H. E. Stanley, *J. Phys. A: Math. Gen.* **12**, 2073 (1979).
 [13] H. Nakanishi and J. Reynolds, *Phys. Lett. A* **71**, 252 (1979).
 [14] M. Yanuka and R. Engelman, *J. Phys. A: Math. Gen.* **23**, L339 (1990).
 [15] Y. Y. Tarasevich and S. C. van der Marck, *Int. J. Mod. Phys. C* **10**, 1193 (1999).

- [16] C. Tsallis and A. C. N. de Magalhães, *Phys. Rep.* **268**, 305 (1996).
- [17] M. I. González, P. M. Centres, W. Lebrecht, A. J. Ramirez-Pastor, and F. Nieto, *Physica A* **392**, 6330 (2013).
- [18] M. I. González, P. M. Centres, W. Lebrecht, and A. J. Ramirez-Pastor, *J. Stat. Mech.* (2016) 093210.
- [19] M. Dolz, F. Nieto, and A. J. Ramirez-Pastor, *Eur. Phys. J. B* **43**, 363 (2005).
- [20] L. S. Ramirez, N. De la Cruz Félix, P. M. Centres, and A. J. Ramirez-Pastor, *J. Stat. Mech.* (2017) 023206.
- [21] H. Harder, A. Bunde, and W. Dieterich, *J. Chem. Phys.* **85**, 4123 (1986).
- [22] H. Holloway, *Phys. Rev. B* **37**, 874 (1988).
- [23] Z. Gao and Z. R. Yang, *Physica A* **255**, 242 (1998).
- [24] Y. Yu. Tarasevich, V. V. Laptev, N. V. Vygornitskii, and N. I. Lebovka, *Phys. Rev. E* **91**, 012109 (2015).
- [25] M. C. Gimenez and A. J. Ramirez-Pastor, *Phys. Rev. E* **94**, 032129 (2016).
- [26] Y. Yu. Tarasevich, A. S. Burmistrov, T. S. Shinyaeva, V. V. Laptev, N. V. Vygornitskii, and N. I. Lebovka, *Phys. Rev. E* **92**, 062142 (2015).
- [27] Lj. Budinski-Petković, I. Lončarević, Z. M. Jakšić, and S. B. Vrhovac, *J. Stat. Mech.* (2016) 053101.
- [28] P. M. Centres and A. J. Ramirez-Pastor, *J. Stat. Mech.* (2015) P10011.
- [29] R. S. Nord and J. W. Evans, *J. Chem. Phys.* **93**, 8397 (1990).
- [30] R. S. Nord, *J. Stat. Comp. Sim.* **39**, 231 (1991).
- [31] J. W. Evans, *Rev. Mod. Phys.* **65**, 1281 (1993).
- [32] J. Hoshen and R. Kopelman, *Phys. Rev. B* **14**, 3438 (1976).
- [33] K. Binder, *Rep. Prog. Phys.* **60**, 487 (1997).
- [34] F. Yonezawa, S. Sakamoto, and M. Hori, *Phys. Rev. B* **40**, 636 (1989).
- [35] F. Yonezawa, S. Sakamoto, and M. Hori, *Phys. Rev. B* **40**, 650 (1989).
- [36] S. Biswas, A. Kundu, and A. K. Chandra, *Phys. Rev. E* **83**, 021109 (2011).
- [37] A. K. Chandra, *Phys. Rev. E* **85**, 021149 (2012).
- [38] M. C. Gimenez, F. Nieto, and A. J. Ramirez-Pastor, *J. Phys. A: Math. Gen.* **38**, 3253 (2005).
- [39] V. Cornette, A. J. Ramirez-Pastor, and F. Nieto, *Physica A* **327**, 71 (2003).
- [40] V. Cornette, A. J. Ramirez-Pastor, and F. Nieto, *Eur. Phys. J. B* **36**, 391 (2003).
- [41] A similar behavior is expected for heterogeneous linear k -mers ($k > 2$).